PHYSICAL REVIEW B **112**, 104208 (2025)

Hydrogen liquid-liquid transition from first principles and machine learning

Giacomo Tenti,[1,*] Bastian Jäckl,[2] Kousuke Nakano,[3,4] Matthias Rupp,[2,5] and Michele Casula[6,†]
[1]*International School for Advanced Studies (SISSA), Via Bonomea 265, 34136 Trieste, Italy*
[2]*Department of Computer and Information Science, University of Konstanz, Box 188, 78457 Konstanz, Germany*
[3]*Center for Basic Research on Materials, National Institute for Materials Science (NIMS), 1-2-1 Sengen, Tsukuba, Ibaraki 305-0047, Japan*
[4]*Center for Emergent Matter Science (CEMS), RIKEN, 2-1 Hirosawa, Wako, Saitama 351-0198, Japan.*
[5]*Scientific Instrumentation and Process Technology unit, Luxembourg Institute of Science and Technology (LIST),*
Maison de l'Innovation, 5 avenue des Hauts-Fourneaux, L-4362 Esch-sur-Alzette, Luxembourg
[6]*Institut de Minéralogie, de Physique des Matériaux et de Cosmochimie (IMPMC), Sorbonne Université,*
CNRS UMR 7590, MNHN, 4 Place Jussieu, 75252 Paris, France

(Received 5 February 2025; revised 23 July 2025; accepted 21 August 2025; published 24 September 2025)

The molecular-to-atomic liquid-liquid transition (LLT) in high-pressure hydrogen is a fundamental topic touching domains from planetary science to materials modeling. Yet, the nature of the LLT is still under debate. To resolve it, numerical simulations must cover length and time scales spanning several orders of magnitude. We overcome these size and time limitations by constructing a fast and accurate machine-learning interatomic potential (MLIP) built on the MACE neural network architecture. The MLIP is trained on Perdew-Burke-Ernzerhof (PBE) density functional calculations and uses a modified loss function correcting for an energy bias in the molecular phase. Classical and path-integral molecular dynamics driven by this MLIP show that the LLT is always supercritical above the melting temperature. The position of the corresponding Widom line agrees with previous *ab initio* PBE calculations, which in contrast predicted a first-order LLT. According to our calculations, the crossover line becomes a first-order transition only inside the molecular crystal region. These results call for a reconsideration of the LLT picture previously drawn.

DOI: 10.1103/pbrk-3zgd

I. INTRODUCTION

Pristine hydrogen is one of the most widely studied materials, both theoretically and experimentally [1]. Indeed, despite being made of the simplest atomic constituent, it exhibits a surprisingly rich phase diagram. The molecular-to-atomic transition happening upon liquid hydrogen compression is crucial for planetary science, in particular for understanding the interior of giant gas planets [2] and their magnetic fields [3]. This liquid-liquid transition (LLT) has been extensively investigated both experimentally [4–14] and via numerical simulations [15–37].

As is often the case for high-pressure hydrogen, experiments based on static [38,39] and dynamic [40] compression give contrasting results, the dynamic experiments predicting a larger transition pressure. Uncertainty is also present in the numerical simulations. Results obtained with *ab initio* molecular dynamics (AIMD) using density functional theory (DFT) show large variability with respect to the choice of the exchange-correlation functional. For instance, the transition pressure can vary by 200 GPa when including long-range van der Waals corrections [41].

The nature of the LLT has been debated, with many first-principles simulations [15,21,22,26,27,30,35] suggesting a first-order LLT below a critical temperature T_c and pressure p_c, based on the observation of kinks in the equation of state (EOS). Given the long correlations in both time and space expected near the transition, the outcome of first-principles molecular dynamics (MD) simulations using DFT or quantum Monte Carlo (QMC) methods has been questioned because of the short time scales and/or the small system sizes considered. This could be reflected in the large variability of the predicted T_c and p_c, which range from $T_c \sim 4000$ K and $p_c \sim 30$ GPa [27,29], to $T_c \sim 1250$ K and $p_c \sim 150$ GPa for the most recent simulations [30].

In the past two decades, large-scale simulations have been made possible by the introduction of machine learning interatomic potentials [42] (MLIPs). These provide results at much lower computational cost, once trained on datasets generated with *ab initio* methods. However, the derivation of an MLIP is a delicate step *per se*, possibly introducing a residual bias. A recent MLIP model, based on the NequIP [43] neural network (NN) and trained on DFT data, gave a T_c value smaller than previous estimates [44]. This model has a pressure bias of about 5 GPa in the EOS, once compared with the corresponding *ab initio* predictions. Recent simulations based on another MLIP trained on the same DFT functional [34] suggested that the LLT is instead a smooth crossover, even though the accuracy of the model has been criticized [35,45].

In this work, we present results for the LLT obtained with MACE [46], a framework combining an equivariant message-passing NN with high-body-order messages, which shows remarkable accuracy compared to other types of MLIPs [47]. In particular, we trained a MACE MLIP on the

---

[*] Contact author: gtenti@sissa.it
[†] Contact author: michele.casula@impmc.upmc.fr

Perdew-Burke-Ernzerhof (PBE) functional and used it to study the nature of the LLT as a function of both system size and simulation length. This also allows us to directly compare our results with the large body of literature that used the same functional [1,18,19,21–23,25,27,29,30,33–35,37,44,45,47]. Our results reveal a first-order transition between an atomic liquid and a molecular solid at low temperatures ($T < 950$ K), due to the melting line proximity. At higher temperatures, our simulations indicate a crossover between molecular and atomic liquids in the thermodynamic limit.

II. MACE MODEL FROM FIRST PRINCIPLES

To overcome the time and size limitations of *ab initio* simulations, while also retaining a high accuracy across the LLT, we constructed a MACE MLIP by applying a correction to the loss function usually minimized to find optimal parameters of the model. During the optimization, the loss and its gradients are evaluated on a subset of training configurations ("batch") of dimension N_b. For the μ-th configuration in the batch, having N_μ atoms, E_μ^{pred}, $\mathbf{F}_{\mu,j}^{\text{pred}}$, and $\boldsymbol{\sigma}_\mu^{\text{pred}}$ are the total energy, the force acting on the j-th atom and the virial stress tensor, respectively, as predicted by the MLIP while E_μ^{ref}, $\mathbf{F}_{\mu,j}^{\text{ref}}$, and $\boldsymbol{\sigma}_\mu^{\text{ref}}$ are the same quantities as calculated with DFT. A standard loss function $\mathcal{L}$ is the weighted sum of the mean squared errors (MSEs) of the different observables:

$$\begin{aligned}\mathcal{L} = {} & w_E \frac{1}{N_b}\sum_{\mu=1}^{N_b}\left[\frac{1}{N_\mu}\left(E_\mu^{\text{pred}} - E_\mu^{\text{ref}}\right)\right]^2 \\ & + w_F \frac{1}{N_b}\sum_{\mu=1}^{N_b}\frac{1}{3N_\mu}\sum_{j=1}^{N_\mu}\sum_{\alpha=x,y,z}\left[F_{\mu,j,\alpha}^{\text{pred}} - F_{\mu,j,\alpha}^{\text{ref}}\right]^2 \\ & + w_\sigma \frac{1}{N_b}\sum_{\mu=1}^{N_b}\frac{1}{9}\sum_{\alpha=x,y,z}\sum_{\beta=x,y,z}\left[\sigma_{\mu,\alpha,\beta}^{\text{pred}} - \sigma_{\mu,\alpha,\beta}^{\text{ref}}\right]^2, \end{aligned} \tag{1}$$

where w_E, w_F, and w_σ are tunable weights. However, when employing the loss in Eq. (1) to train the model [48], we noticed the appearance of molecular solid-like structures at high temperatures ($T \sim 1200$ K) during the dynamics. AIMD simulations at the same conditions and system sizes show how these configurations are not dynamically stable, and, therefore, are an artifact of the model. Even after the inclusion of these structures in the training set, the standard loss function still energetically favored these configurations (see Ref. [49] for details). The atomic phase, on the other hand, seemed to be described correctly.

An analysis of the partial energy error distributions for this model, computed on subsets of the training set describing the selected phases, reveals how the loss function $\mathcal{L}$ produces a bias, i.e., a nonzero mean of $E_\mu^{\text{pred}} - E_\mu^{\text{ref}}$. Indeed, being a function of the MSEs, $\mathcal{L}$ only guarantees that the total error distribution is centered around zero.

With this in mind, we modified the loss function by including a term that penalizes a global energy bias in the prediction error on the subset of *molecular configurations*, thus improving the description of this phase. Specifically, we used the modified loss $\mathcal{L}' = \mathcal{L} + \Delta\mathcal{L}$ with

$$\Delta\mathcal{L} = w_E \lambda \frac{1}{N_\text{b}}\left|\sum_{\mu\in\text{mol}}\frac{1}{N_\mu}\left(E_\mu^{\text{pred}} - E_\mu^{\text{ref}}\right)\right|, \tag{2}$$

where λ is a parameter controlling the relative weight of the penalty with respect to the energy term of the standard loss function, w_E is the same hyperparameter as in Eq. (1), and the sum only considers molecular configurations in a given training batch. To classify configurations as either atomic or molecular, we used a static criterion that solely depends on atomic positions: A configuration is classified as molecular if the first peak of its radial distribution function $g(r)$ [estimated by fitting the $g(r)$ with a Gaussian function for $r \in [0, 1.3]$ Å] is larger than a threshold, here set to 1.8.

TABLE I. Root mean squared errors of the final MACE MLIP for the energy per atom (RMSE$_E$) and the forces (RMSE$_F$) on the training, validation, and test sets.

	RMSE$_E$ (meV/atom)	RMSE$_F$ (meV/Å)
Training	2.2	116
Validation	2.1	118
Test	2.0	116

We observed that the models trained using $\mathcal{L}'$ have a much smaller energy error for the molecular solid-like structures, which do not appear anymore during the dynamics at high temperatures. As a consequence of the modified loss, the energy error distribution on the training set is slightly altered, with relative energies between different types of structures in much better agreement with respect to the *ab initio* PBE reference values, as discussed in Ref. [49].

To train the final MLIP, we compiled a dataset of 21 812 configurations. We extracted ~17 000 configurations of 128 hydrogen atoms each from the MD simulations of Refs. [50] and [51] (see Ref. [49] for the density-temperature distribution of this set). An additional set of 3000 128-atoms configurations was selected from a series of AIMD simulations at lower temperatures (800 and 900 K). We also added 500 snapshots with 256 and 512 atoms extracted from MD runs with early iterations of the MACE model. Finally, we included solid structures (see Ref. [52]) and ~100 low-temperature 96-atom configurations from Ref. [53]. To ensure consistency across the dataset, we recomputed energies, forces, and pressures at the PBE level, using the QUANTUM ESPRESSO package [54–56]. A projector augmented-wave (PAW) pseudopotential [57] together with a 60 Ry plane-waves cutoff was used. A sufficiently dense **k**-point grid for each system size was employed to cure finite-size effects. For instance, we used a 4×4×4 grid for the configurations with 128 atoms.

From this dataset, we randomly extracted 280 configurations for testing. From the remaining configurations, 95% were used for training, and 5% for validation. This last group of configurations is used during the training to assess the performance of the model. At the end of the optimization, the best model is selected as the one minimizing the loss on the validation set.

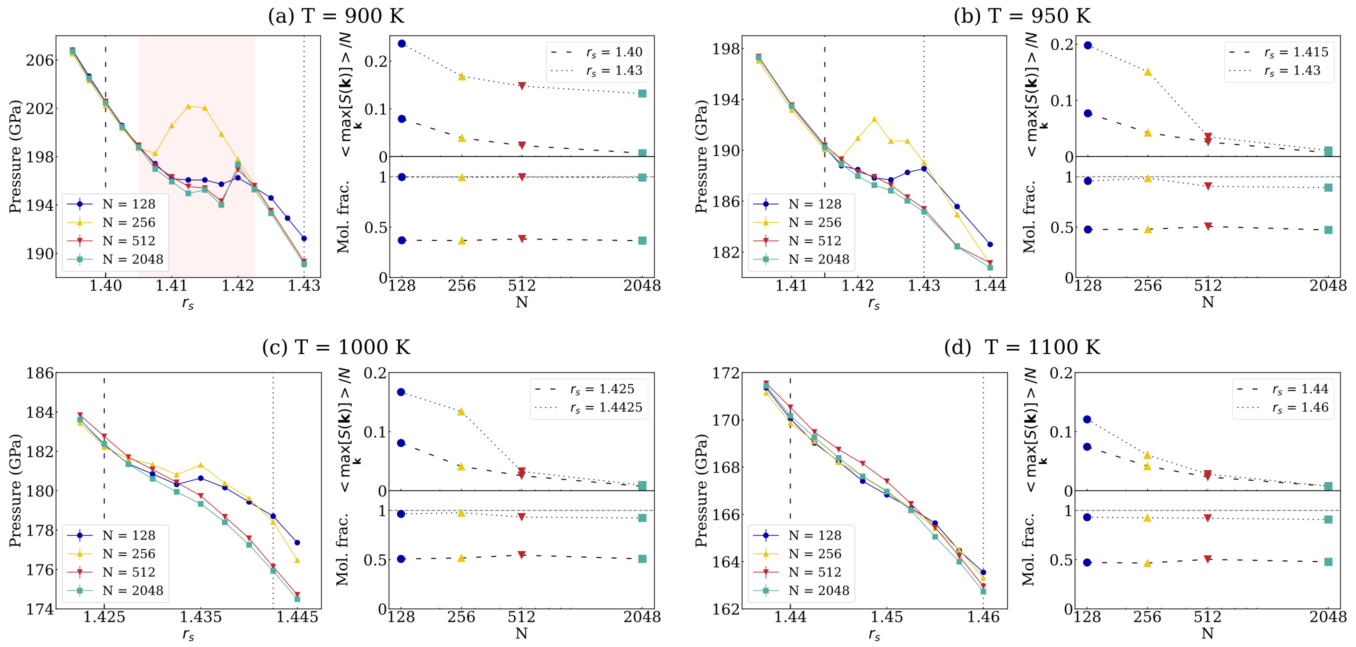

FIG. 1. Results for MD simulations obtained with the MACE model for different temperatures: (a) $T = 900$, (b) 950, (c) 1000, and (d) 1100 K. For each temperature, the left panel reports the EOS close to the LLT for the different system sizes. For $T = 900$ K the red shaded area highlights the r_s range for which hysteresis is observed at all values of N. The right panels show the average $\max_{\mathbf{k}} S(\mathbf{k})/N$ along the trajectory (top right) and the average molecular fraction m (bottom right) as a function of the system size N for two different values of the Wigner-Seitz radius r_s.

Table I reports the accuracy of this MACE model, measured by the root mean squared error (RMSE) on the energy per atom and the forces on the training, validation, and test sets. The test-set RMSE for the virial pressure is ∼1 GPa. Compared to the MLIP proposed in Ref. [34], our model has an error on energy 6–7 times smaller and is twice as accurate on forces. The recent NequIP model of Ref. [44] shows a very similar RMSE on energy, but has a 40% larger RMSE on forces.

III. LLT SIMULATIONS: FINITE-SIZE SCALING

The computational efficiency of the MACE model enabled us to study the behavior of the LLT as a function of both temperature and system size. We ran MD simulations in the NVT ensemble using the LAMMPS code [58] interfaced with MACE. We considered systems with $N = 128$, 256, 512, and 2048 hydrogen atoms treated as classical nuclei, and cubic supercells. We performed simulations as long as 0.6 ns, about two orders of magnitude longer than what is usually achieved with AIMD. For the dynamics, we used a time step of 0.2 fs and controlled the temperature via the stochastic velocity rescaling scheme [59], with a characteristic time of $\tau = 0.1$ ps.

To accurately study the nature of the transition, we calculated the EOS of the system in the vicinity of the LLT, using a dense grid of Wigner-Seitz radii r_s, where $\frac{4\pi}{3}(r_s a_0)^3 = \frac{V}{N}$ with V and a_0 being the system volume and the Bohr radius, respectively. The results are presented in Fig. 1 for four different temperatures in the [900–1100] K range. From the EOS, we can identify three distinct regimes for the LLT. At the lowest temperature computed here, i.e., $T = 900$ K [Fig. 1(a)], the model clearly predicts a first-order transition, signaled by the hysteresis present in the EOS for all system sizes. At $T = 950$ and 1000 K [Figs. 1(b) and 1(c), respectively], the EOS has a strong dependence on the system size in the transition region: the smaller systems (i.e., $N = 128$ and 256) suggest again a first-order transition, while for larger N the pressure plateau and hysteresis are missing. Finally, at $T \geqslant 1100$ K [Fig. 1(d)] the results indicate a smooth crossover, with a relatively small size dependence.

To characterize the LLT, the sole observation of the EOS is not sufficient, since it is known that for these transitions the density is not the primary order parameter [60]. In particular, we computed the stable molecular fraction [23,30,47] of the system, defined in this case as the average number of hydrogen pairs whose constituent atoms stay within a distance of 1.05 Å for at least a time $\tau \sim 80$ fs.

The results corresponding to r_s values slightly before/after the transition are also shown in Fig. 1. In all cases, the molecular fraction rapidly increases from values around 0.5 to values close to 1, signaling an atomic-to-molecular transition as r_s increases.

Besides the stable molecular fraction, we also computed the structure factor to detect long-range spatial correlations, i.e.,

$$S(\mathbf{k}) = \left\langle \frac{1}{N} \sum_{i,j} \exp(i\mathbf{k} \cdot (\mathbf{R}_i - \mathbf{R}_j)) \right\rangle,$$

where $\langle \cdots \rangle$ indicates the average over the trajectory, $\mathbf{R}_1, \ldots, \mathbf{R}_N$ are atom positions, and $\mathbf{k} = \frac{2\pi}{L}(n_1, n_2, n_3)$, with L being the side of the cubic simulation box and n_1, n_2, n_3 integer numbers. In particular, the maximum value of $S(\mathbf{k})$ can be used as a proxy for the formation of crystalline structures, with $\max_{\mathbf{k}} S(\mathbf{k}) \propto N$ in a solid system in the thermodynamic limit. On the contrary, in a liquid, the rotational invariance implies that the contribution of each $\mathbf{k}$ to the $S(\mathbf{k})$ will stay constant for $N \to \infty$. The value of the average $\max_{\mathbf{k}} S(\mathbf{k})/N$ as a function of the number of particles is reported in the top right panels of Fig. 1. In the atomic phase, our simulations show that the system is a liquid at all temperatures. In the molecular region, the behavior of $\max_{\mathbf{k}} S(\mathbf{k})/N$ is instead strongly temperature dependent. Interestingly, the first-order transition observed in the EOS at $T = 900$ K is accompanied by a nonvanishing value of $\max_{\mathbf{k}} S(\mathbf{k})/N$ in the thermodynamic limit, revealing a long-range spatial order of the molecular phase at this temperature [Fig. 1(a)]. Moreover, at $T = 950$ and 1000 K, a large value of $\max_{\mathbf{k}} S(\mathbf{k})/N$ is present for $N = 128$ and 256 on the molecular side, then vanishing at larger N [Figs. 1(b) and 1(c)]. This suggests that the first-order transition seen in smaller systems is due to finite-size effects and it is between a molecular crystal and an atomic liquid. A genuine molecular liquid is instead observed for all system sizes at temperature $T \geqslant 1100$ K [Fig. 1(d)].

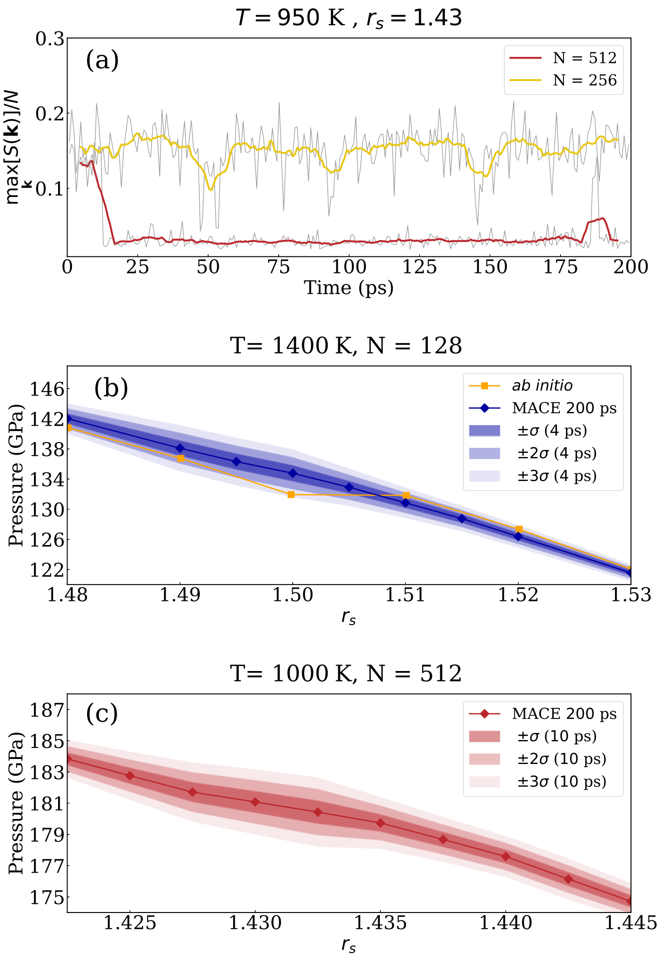

FIG. 2. (a) Value of $\max_{\mathbf{k}} S(\mathbf{k})/N$ as a function of the simulation time for two systems, with $N = 256$ and $N = 512$ atoms, respectively, at temperature $T = 950$ K and $r_s = 1.43$. Colored lines represent running averages over a time window of 8 ps. (b) Results for 200 ps long simulations, $N = 128$, $T = 1400$ K and corresponding confidence intervals, estimated from a running average with time window $\tau_{\text{run}} = 4$ ps. The AIMD result reported in Ref. [50] is also shown. (c) Same as (b) but with $N = 512$, $T = 1000$ K, and $\tau_{\text{run}} = 10$ ps.

IV. LLT SIMULATIONS: FINITE-TIME EFFECTS

Our finite-size scaling analysis highlights the importance of considering sufficiently large systems to obtain converged results for the LLT. This is further demonstrated in Fig. 2(a), where the behavior of $\max_{\mathbf{k}} S(\mathbf{k})/N$ is plotted as a function of the simulation time for two sizes, namely $N = 256$ and 512, at $T = 950$ K and $r_s = 1.43$. While the smaller system is in a solid-like state for the majority of the time, the system with $N = 512$ occasionally crystallizes, as indicated by the two jumps of $\max_{\mathbf{k}} S(\mathbf{k})/N$ at the beginning and the end of the MD run, but mostly remains liquid. This behavior not only confirms the size dependence already seen, but also shows that at least 10 ps are necessary to melt the crystal for $N = 512$, suggesting that ∼100 ps are needed to obtain fully converged results near the transition.

To analyze the possibility that the kinks identified in the EOS of previous AIMD results originate from the short length of these simulations, we analyzed 0.2 ns long trajectories obtained with the MACE model for values of r_s close to the transition at different temperatures above our T_c. The results are shown in Figs. 2(b) and 2(c) for the system of $N = 128$ at $T = 1400$ K and the one of $N = 512$ at $T = 1000$ K, respectively. Using long trajectories, we computed the pressure running average using a variable-size time window τ_{run}, corresponding to simulation times achievable by AIMD, e.g., $\tau_{\text{run}} \sim 10$ ps. The variance of the running average gives an idea of the variability of the estimated equilibrium pressure when running MD simulations of length equal to τ_{run}. From Figs. 2(b) and 2(c), the estimated variance grows in the vicinity of the transition, and the presence of a pressure plateau in the EOS can be understood as an artifact due to the lack of phase-space sampling.

For the smallest system [$N = 128$, Fig. 2(b)], we also compared our results with the PBE AIMD ones reported in Ref. [50] at $T = 1400$ K for the same size. The pressure plateau here is within the 3σ uncertainty region estimated from a running average of 4 ps, slightly longer than the average length of the AIMD simulations. The results at lower temperature $T = 1000$ K for a larger system of 512 atoms [Fig. 2(c)] show that even a 10 ps long dynamics can, in principle, produce artificial kinks of the size reported in the literature [21,30]. Even though, in principle, this estimation depends on the algorithmic details, such as the choice of the thermostat, we do not expect this to change our conclusions.

V. WIDOM LINE

Both the first-order transition and the crossover above the critical temperature T_c can be further characterized by studying the behavior of the isochoric specific heat (i.e., the heat capacity per particle), $c_v = \frac{1}{N k_B T^2}(\langle E^2\rangle - \langle E\rangle^2)$, as a function of temperature, density, and system size. The results for c_v obtained from simulations with $N = 2048$ hydrogen atoms at temperatures up to 1800 K are reported in Fig. 3. For each temperature, we estimated the location and value of the maximum. For temperatures between 900 K and 1100 K, we

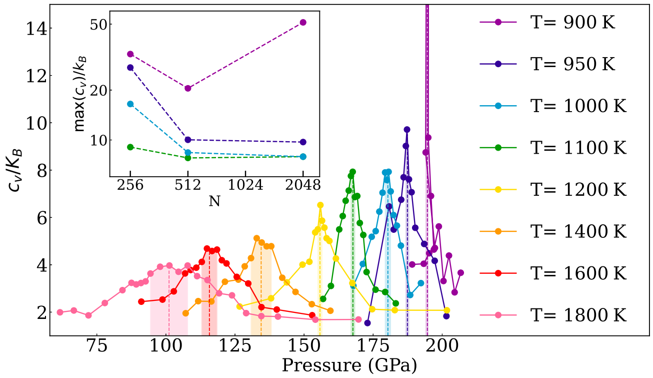

FIG. 3. Specific heat per particle vs pressure along the isotherms, for $N = 2048$ obtained with the MACE model. The shaded areas indicate the uncertainty in the peak position. In the inset, we report the size scaling of the maximum of c_v/k_B for four different temperatures (in a log-log scale). The results confirm a first-order transition for $T = 900$ K, where c_v scales with a behavior close to linear, and a smooth crossover for higher temperatures in the thermodynamic limit.

also studied the size scaling of the c_v maximum, as shown in the inset of Fig. 3. In a first-order transition, the c_v peak presents a divergence scaling like $\sim N$ in the thermodynamic limit [61]. As shown in the figure, linear scaling is observed at $T = 900$ K, while c_v tends to a constant for higher temperatures. This is consistent with our EOS results locating the critical point between $T = 900$ and 950 K. The position of the c_v maximum at higher temperatures allows one to determine the Widom line in the supercritical region. The results are reported in Fig. 4. Our Widom line shows remarkable agreement with previous simulations of the LLT obtained with the PBE functional. In particular, our results well reproduce the ones reported in Ref. [21] for temperatures up to 1400 K and those of Ref. [35] for higher temperatures, even though they do not agree on the LLT first-order character for $T \geqslant 900$ K.

VI. CONCLUSIONS

Enabled by an accurate and efficient MLIP based on the MACE architecture, we show that the LLT between molecular and atomic hydrogen is always supercritical above the melting temperature. For this, we performed NVT MD simulations in a temperature range between 900 and 1800 K of systems with up to 2048 hydrogen atoms and simulation times of up to 600 ps. We preserved the *ab initio* PBE quality of the MACE model across the transition by virtue of a modified loss function, yielding consistent energy differences between atomic and molecular configurations.

For temperatures above 900 K, the MACE model predicts a proper LLT in the thermodynamic limit ($N \geqslant 512$), which turns out to be a smooth crossover. Up to $T = 1000$ K, defective crystal structures are observed for small systems due to strong finite-size effects, giving rise to a first-order transition that disappears as N increases.

At the lowest temperature (900 K), the model predicts a first-order transition in the thermodynamic limit. The structure factor analysis reveals the presence of long-range spatial order in the molecular phase, showing that this is a transition between a molecular solid-like system, frustrated by the cubic cell, and an atomic liquid. This transition point lies exactly on the PBE melting line of Ref. [53] (see Fig. 4), calculated with an NN MLIP obtained using the DeePMD package [62], suggesting that the LLT might become first-order inside the crystal region for $T \leqslant 900$ K.

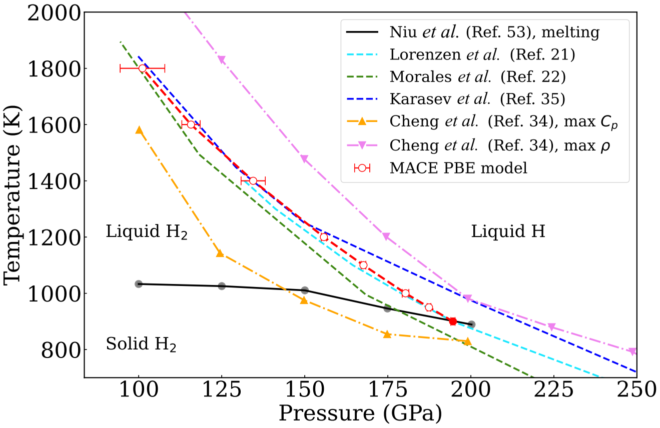

FIG. 4. Classical PBE-LLT location as computed with different methods. AIMD results by Ref. [21] (light blue dashed line), Ref. [22] (green dashed line), and Ref. [35] (blue dashed line). The results for the molecular-to-atomic crossover obtained with an NN MLIP by Ref. [34] are reported with orange and violet markers, corresponding to the maximum of the isobaric specific heat and density, respectively. The black markers and line indicate the recently proposed PBE melting line by Ref. [53], obtained with an NN MLIP and the two-phase method. The MACE model results are indicated with red markers. The filled point at $T = 900$ K indicates the first-order character of the transition, while the empty points correspond to the location of the Widom line given by the c_v maximum (see Fig. 3).

The physical picture provided by the MACE model qualitatively agrees with Ref. [34] on the supercritical nature of the LLT, even though their model could not accurately reproduce the crystallization regime, and predicted a Widom line (estimated from the maximum of the isobaric specific heat c_p) far from the AIMD results (see Fig. 4). The first-order character of the transition observed in other studies may be explained by the large fluctuations expected close to the Widom line, which could lead to the incorrect identification of density jumps and pressure plateaux in the EOS for too short simulation times. Additional path integral MD simulations carried out with the MACE model indicate that the conclusions about the crossover nature of the LLT are not changed by the inclusion of nuclear quantum effects, as reported in Ref. [49].

These results urgently call for a reinvestigation of the LLT using *ab initio* methods beyond DFT, such as QMC. The Δ-learning scheme [50,51] combined with the present MACE model taken as baseline could allow one to access unprecedented system sizes and simulation lengths, by extending this work to QMC-based MLIP applications.

ACKNOWLEDGMENTS

K.N. acknowledges financial support from MEXT Leading Initiative for Excellent Young Researchers (Grant No.

JPMXS0320220025) and from by JST BOOST (Grant No. JPMJBY24F3). B.J. acknowledges support by the state of Baden-Württemberg through bwHPC. M.C. thanks the European High Performance Computing Joint Undertaking (JU) for the partial support through the "EU-Japan Alliance in HPC" HANAMI project (Hpc AlliaNce for Applications and supercoMputing Innovation: the Europe - Japan collaboration) under the contract HORIZON-EUROHPC-JU-2022-INCO-04. This work has received funding from the European Center of Excellence in Exascale Computing TREX (Targeting Real chemical accuracy at the Exascale, grant 952165). The authors acknowledge discussions with David Ceperley, Michele Ceriotti, Gábor Csányi, Carlo Pierleoni, Thomas Bischoff, Marco Cherubini, and Abhishek Raghav. M.C. acknowledges GENCI for providing computational resources on the CEA-TGCC Irene and IDRIS Jean-Zay supercomputer clusters under project number A0170906493 and the TGCC special session.

DATA AVAILABILITY

The data that support the findings of this article are openly available [63,64].

[1] M. Bonitz, J. Vorberger, M. Bethkenhagen, M. P. Böhme, D. M. Ceperley, A. Filinov, T. Gawne, F. Graziani, G. Gregori, P. Hamann, S. B. Hansen, M. Holzmann, S. X. Hu, H. Kählert, V. V. Karasiev, U. Kleinschmidt, L. Kordts, C. Makait, B. Militzer, Z. A. Moldabekov *et al.*, Toward first principles-based simulations of dense hydrogen, Phys. Plasmas **31**, 110501 (2024).

[2] R. Helled, G. Mazzola, and R. Redmer, Understanding dense hydrogen at planetary conditions, Nat. Rev. Phys. **2**, 562 (2020).

[3] J. E. P. Connerney, M. Benn, J. B. Bjarno, T. Denver, J. Espley, J. L. Jorgensen, P. S. Jorgensen, P. Lawton, A. Malinnikova, J. M. Merayo, S. Murphy, J. Odom, R. Oliversen, R. Schnurr, D. Sheppard, and E. J. Smith, The juno magnetic field investigation, Space Sci. Rev. **213**, 39 (2017).

[4] S. T. Weir, A. C. Mitchell, and W. J. Nellis, Metallization of fluid molecular hydrogen at 140 GPa (1.4 Mbar), Phys. Rev. Lett. **76**, 1860 (1996).

[5] V. E. Fortov, R. I. Ilkaev, V. A. Arinin, V. V. Burtzev, V. A. Golubev, I. L. Iosilevskiy, V. V. Khrustalev, A. L. Mikhailov, M. A. Mochalov, V. Y. Ternovoi, and M. V. Zhernokletov, Phase transition in a strongly nonideal deuterium plasma generated by quasi-isentropical compression at megabar pressures, Phys. Rev. Lett. **99**, 185001 (2007).

[6] V. Dzyabura, M. Zaghoo, and I. F. Silvera, Evidence of a liquid–liquid phase transition in hot dense hydrogen, Proc. Natl. Acad. Sci. USA **110**, 8040 (2013).

[7] K. Ohta, K. Ichimaru, M. Einaga, S. Kawaguchi, K. Shimizu, T. Matsuoka, N. Hirao, and Y. Ohishi, Phase boundary of hot dense fluid hydrogen, Sci. Rep. **5**, 16560 (2015).

[8] M. D. Knudson, M. P. Desjarlais, A. Becker, R. W. Lemke, K. R. Cochrane, M. E. Savage, D. E. Bliss, T. R. Mattsson, and R. Redmer, Direct observation of an abrupt insulator-to-metal transition in dense liquid deuterium, Science **348**, 1455 (2015).

[9] R. S. McWilliams, D. A. Dalton, M. F. Mahmood, and A. F. Goncharov, Optical properties of fluid hydrogen at the transition to a conducting state, Phys. Rev. Lett. **116**, 255501 (2016).

[10] M. Zaghoo, A. Salamat, and I. F. Silvera, Evidence of a first-order phase transition to metallic hydrogen, Phys. Rev. B **93**, 155128 (2016).

[11] M. Zaghoo and I. F. Silvera, Conductivity and dissociation in liquid metallic hydrogen and implications for planetary interiors, Proc. Natl. Acad. Sci. USA **114**, 11873 (2017).

[12] M. Zaghoo, R. J. Husband, and I. F. Silvera, Striking isotope effect on the metallization phase lines of liquid hydrogen and deuterium, Phys. Rev. B **98**, 104102 (2018).

[13] P. M. Celliers, M. Millot, S. Brygoo, R. S. McWilliams, D. E. Fratanduono, J. R. Rygg, A. F. Goncharov, P. Loubeyre, J. H. Eggert, J. L. Peterson, N. B. Meezan, S. L. Pape, G. W. Collins, R. Jeanloz, and R. J. Hemley, Insulator-metal transition in dense fluid deuterium, Science **361**, 677 (2018).

[14] S. Jiang, N. Holtgrewe, Z. M. Geballe, S. S. Lobanov, M. F. Mahmood, R. S. McWilliams, and A. F. Goncharov, A spectroscopic study of the insulator–metal transition in liquid hydrogen and deuterium, Adv. Sci. **7**, 1901668 (2020).

[15] S. Scandolo, Liquid–liquid phase transition in compressed hydrogen from first-principles simulations, Proc. Natl. Acad. Sci. USA **100**, 3051 (2003).

[16] S. A. Bonev, B. Militzer, and G. Galli, Ab initio simulations of dense liquid deuterium: Comparison with gas-gun shock-wave experiments, Phys. Rev. B **69**, 014101 (2004).

[17] K. T. Delaney, C. Pierleoni, and D. M. Ceperley, Quantum Monte Carlo simulation of the high-pressure molecular-atomic crossover in fluid hydrogen, Phys. Rev. Lett. **97**, 235702 (2006).

[18] J. Vorberger, I. Tamblyn, B. Militzer, and S. A. Bonev, Hydrogen-helium mixtures in the interiors of giant planets, Phys. Rev. B **75**, 024206 (2007).

[19] B. Holst, R. Redmer, and M. P. Desjarlais, Thermophysical properties of warm dense hydrogen using quantum molecular dynamics simulations, Phys. Rev. B **77**, 184201 (2008).

[20] C. Attaccalite and S. Sorella, Stable liquid hydrogen at high pressure by a novel *ab initio* molecular-dynamics calculation, Phys. Rev. Lett. **100**, 114501 (2008).

[21] W. Lorenzen, B. Holst, and R. Redmer, First-order liquid-liquid phase transition in dense hydrogen, Phys. Rev. B **82**, 195107 (2010).

[22] M. A. Morales, C. Pierleoni, E. Schwegler, and D. M. Ceperley, Evidence for a first-order liquid-liquid transition in high-pressure hydrogen from ab initio simulations, Proc. Natl. Acad. Sci. USA **107**, 12799 (2010).

[23] I. Tamblyn and S. A. Bonev, Structure and phase boundaries of compressed liquid hydrogen, Phys. Rev. Lett. **104**, 065702 (2010).

[24] G. Mazzola, S. Yunoki, and S. Sorella, Unexpectedly high pressure for molecular dissociation in liquid hydrogen by electronic simulation, Nat. Commun. **5**, 3487 (2014).

[25] J. Yang, C. L. Tian, F. S. Liu, L. C. Cai, H. K. Yuan, M. M. Zhong, and F. Xiao, A new evidence of first-order phase transition for hydrogen at 3000 K, Europhys. Lett. **109**, 36003 (2015).

[26] C. Pierleoni, M. A. Morales, G. Rillo, M. Holzmann, and D. M. Ceperley, Liquid–liquid phase transition in hydrogen by

coupled electron–ion Monte Carlo simulations, Proc. Natl. Acad. Sci. USA **113**, 4953 (2016).

[27] G. E. Norman and I. M. Saitov, Critical point and mechanism of the fluid–fluid phase transition in warm dense hydrogen, Doklady Physics **62**, 294 (2017).

[28] G. Mazzola, R. Helled, and S. Sorella, Phase diagram of hydrogen and a hydrogen-helium mixture at planetary conditions by quantum Monte Carlo simulations, Phys. Rev. Lett. **120**, 025701 (2018).

[29] C. Tian, F. Liu, H. Yuan, H. Chen, and A. Kuan, First-order liquid-liquid phase transition in compressed hydrogen and critical point, J. Chem. Phys. **150**, 204114 (2019).

[30] H. Y. Geng, Q. Wu, M. Marqués, and G. J. Ackland, Thermodynamic anomalies and three distinct liquid-liquid transitions in warm dense liquid hydrogen, Phys. Rev. B **100**, 134109 (2019).

[31] G. Rillo, M. A. Morales, D. M. Ceperley, and C. Pierleoni, Optical properties of high-pressure fluid hydrogen across molecular dissociation, Proc. Natl. Acad. Sci. USA **116**, 9770 (2019).

[32] J. Hinz, V. V. Karasiev, S. X. Hu, M. Zaghoo, D. Mejía-Rodríguez, S. B. Trickey, and L. Calderín, Fully consistent density functional theory determination of the insulator-metal transition boundary in warm dense hydrogen, Phys. Rev. Res. **2**, 032065(R) (2020).

[33] T. Bryk, C. Pierleoni, G. Ruocco, and A. P. Seitsonen, Characterization of molecular-atomic transformation in fluid hydrogen under pressure via long-wavelength asymptote of charge density fluctuations, J. Mol. Liq. **312**, 113274 (2020).

[34] B. Cheng, G. Mazzola, C. J. Pickard, and M. Ceriotti, Evidence for supercritical behaviour of high-pressure liquid hydrogen, Nature (London) **585**, 217 (2020).

[35] V. V. Karasiev, J. Hinz, S. Hu, and S. Trickey, On the liquid–liquid phase transition of dense hydrogen, Nature (London) **600**, E12 (2021).

[36] A. Bergermann, L. Kleindienst, and R. Redmer, Nonmetal-to-metal transition in liquid hydrogen using density functional theory and the Heyd–Scuseria–Ernzerhof exchange-correlation functional, J. Chem. Phys. **161**, 234303 (2024).

[37] G. Gliaudelis, V. Lukyanchuk, N. Chtchelkatchev, I. Saitov, and N. Kondratyuk, Dynamical properties of hydrogen fluid at high pressures, J. Chem. Phys. **162**, 024504 (2025).

[38] A. F. Goncharov, I. I. Mazin, J. H. Eggert, R. J. Hemley, and H.-K. Mao, Invariant points and phase transitions in deuterium at megabar pressures, Phys. Rev. Lett. **75**, 2514 (1995).

[39] W. A. Bassett, Diamond anvil cell, 50th birthday, High Press. Res. **29**, 163 (2009).

[40] W. J. Nellis, Dynamic compression of materials: Metallization of fluid hydrogen at high pressures, Rep. Prog. Phys. **69**, 1479 (2006).

[41] M. A. Morales, R. Clay, C. Pierleoni, and D. M. Ceperley, First principles methods: A perspective from quantum Monte Carlo, Entropy **16**, 287 (2014).

[42] J. Behler, Perspective: Machine learning potentials for atomistic simulations, J. Chem. Phys. **145**, 170901 (2016).

[43] S. Batzner, A. Musaelian, L. Sun, M. Geiger, J. P. Mailoa, M. Kornbluth, N. Molinari, T. E. Smidt, and B. Kozinsky, E(3)-equivariant graph neural networks for data-efficient and accurate interatomic potentials, Nat. Commun. **13**, 2453 (2022).

[44] M. Istas, S. Jensen, Y. Yang, M. Holzmann, C. Pierleoni, and D. M. Ceperley, Liquid-liquid phase transition of hydrogen and its critical point: Analysis from ab initio simulation and a machine-learned potential, Phys. Rev. E **111**, 045307 (2025).

[45] B. Cheng, G. Mazzola, C. J. Pickard, and M. Ceriotti, Reply to: On the liquid–liquid phase transition of dense hydrogen, Nature (London) **600**, E15 (2021).

[46] I. Batatia, D. P. Kovacs, G. Simm, C. Ortner, and G. Csanyi, Mace: Higher order equivariant message passing neural networks for fast and accurate force fields, in *Advances in Neural Information Processing Systems*, edited by S. Koyejo, S. Mohamed, A. Agarwal, D. Belgrave, K. Cho, and A. Oh (Curran Associates, 2022), Vol. 35, pp. 11423–11436.

[47] T. Bischoff, B. Jäckl, and M. Rupp, Hydrogen under Pressure as a Benchmark for Machine-Learning Interatomic Potentials, arXiv:2409.13390.

[48] For building the model, we used 128 equivariant messages, a correlation order of 3, and a cutoff radius of $r_c = 3$ Å.

[49] See Supplemental Material at http://link.aps.org/supplemental/10.1103/pbrk-3zgd for further details about the training of the MACE model, a comparison between the error distribution of two models trained using the standard and modified loss, an analysis of the defective solid found in our simulations, a discussion of the path integral molecular dynamics results, and a comparison between our results and those obtained from ab initio molecular dynamics. (See references [26,35,47,50,51,53,65–67] therein).

[50] A. Tirelli, G. Tenti, K. Nakano, and S. Sorella, High-pressure hydrogen by machine learning and quantum Monte Carlo, Phys. Rev. B **106**, L041105 (2022).

[51] G. Tenti, K. Nakano, A. Tirelli, S. Sorella, and M. Casula, Principal deuterium Hugoniot via quantum Monte Carlo and Δ-learning, Phys. Rev. B **110**, L041107 (2024).

[52] L. Monacelli, M. Casula, K. Nakano, S. Sorella, and F. Mauri, Quantum phase diagram of high-pressure hydrogen, Nat. Phys. **19**, 845 (2023).

[53] H. Niu, Y. Yang, S. Jensen, M. Holzmann, C. Pierleoni, and D. M. Ceperley, Stable solid molecular hydrogen above 900 K from a machine-learned potential trained with diffusion quantum Monte Carlo, Phys. Rev. Lett. **130**, 076102 (2023).

[54] P. Giannozzi, S. Baroni, N. Bonini, M. Calandra, R. Car, C. Cavazzoni, D. Ceresoli, G. L. Chiarotti, M. Cococcioni, I. Dabo, A. D. Corso, S. de Gironcoli, S. Fabris, G. Fratesi, R. Gebauer, U. Gerstmann, C. Gougoussis, A. Kokalj, M. Lazzeri, L. Martin-Samos *et al.*, QUANTUM ESPRESSO: A modular and open-source software project for quantum simulations of materials, J. Phys.: Condens. Matter **21**, 395502 (2009).

[55] P. Giannozzi, O. Andreussi, T. Brumme, O. Bunau, M. B. Nardelli, M. Calandra, R. Car, C. Cavazzoni, D. Ceresoli, M. Cococcioni, N. Colonna, I. Carnimeo, A. D. Corso, S. de Gironcoli, P. Delugas, R. A. DiStasio, A. Ferretti, A. Floris, G. Fratesi, G. Fugallo *et al.*, Advanced capabilities for materials modelling with QUANTUM ESPRESSO, J. Phys.: Condens. Matter **29**, 465901 (2017).

[56] P. Giannozzi, O. Baseggio, P. Bonfà, D. Brunato, R. Car, I. Carnimeo, C. Cavazzoni, S. de Gironcoli, P. Delugas, F. Ferrari Ruffino, A. Ferretti, N. Marzari, I. Timrov, A. Urru, and S. Baroni, QUANTUM ESPRESSO toward the exascale, J. Chem. Phys. **152**, 154105 (2020).

[57] H.PBEK-JPAW_PSL.1.0.0.UPF pseudopotentials available at http://pseudopotentials.quantum-espresso.org/legacy_tables/ps-library/h.

[58] A. P. Thompson, H. M. Aktulga, R. Berger, D. S. Bolintineanu, W. M. Brown, P. S. Crozier, P. J. in 't Veld, A. Kohlmeyer, S. G. Moore, T. D. Nguyen, R. Shan, M. J. Stevens, J. Tranchida, C. Trott, and S. J. Plimpton, LAMMPS—A flexible simulation tool for particle-based materials modeling at the atomic, meso, and continuum scales, Comput. Phys. Commun. **271**, 108171 (2022).

[59] G. Bussi, D. Donadio, and M. Parrinello, Canonical sampling through velocity rescaling, J. Chem. Phys. **126**, 014101 (2007).

[60] H. Tanaka, Liquid–liquid transition and polyamorphism, J. Chem. Phys. **153**, 130901 (2020).

[61] K. Binder, Theory of first-order phase transitions, Rep. Prog. Phys. **50**, 783 (1987).

[62] J. Zeng, D. Zhang, D. Lu, P. Mo, Z. Li, Y. Chen, M. Rynik, L. Huang, Z. Li, S. Shi, Y. Wang, H. Ye, P. Tuo, J. Yang, Y. Ding, Y. Li, D. Tisi, Q. Zeng, H. Bao, Y. Xia *et al.*, DeePMD-kit v2: A software package for deep potential models, J. Chem. Phys. **159**, 054801 (2023).

[63] G. Tenti, https://github.com/giacomotenti/mace (2025).

[64] G. Tenti, B. Jäckl, K. Nakano, M. Rupp, and M. Casula, Additional data for "Hydrogen liquid-liquid transition from first principles and machine learning," Zenodo (2025), doi: 10.5281/zenodo.14790036.

[65] D. P. Kingma and J. Ba, Adam: A method for stochastic optimization, in *Proceedings of the 3rd International Conference on Learning Representations (ICLR)*, edited by Y. Bengio and Y. LeCun (San Diego, California, USA, 2015).

[66] K. Momma and F. Izumi, *VESTA*: A three-dimensional visualization system for electronic and structural analysis, J. Appl. Cryst. **41**, 653 (2008).

[67] F. Mouhat, S. Sorella, R. Vuilleumier, A. M. Saitta, and M. Casula, Fully quantum description of the Zundel ion: Combining variational quantum Monte Carlo with path integral Langevin dynamics, J. Chem. Theory Comput. **13**, 2400 (2017).